

A hybrid framework for forecasting circular excavation collapse: combining physics-based and data-driven modelling

Brian B. Sheil¹

¹RAEng Research Fellow, Department of Engineering Science, University of Oxford, U.K.

Email: brian.sheil@eng.ox.ac.uk. Tel.: 01 865 2 73170

ABSTRACT

The use of supporting fluids to stabilise excavations is a common technique adopted in the construction industry. Rapid detection of incipient collapse for deep excavations and timely decision making are crucial to ensure safety during construction. This paper explores a hybrid framework for forecasting the collapse of fluid-supported circular excavations by combining physics-based and data-driven modelling. Finite element limit analysis is first used to develop a numerical database of stability numbers for both unsupported and fluid-supported circular excavations. The parameters considered in the modelling include excavation geometry, soil strength profile and support fluid properties. A data-driven algorithm is used to 'learn' the numerical results to develop a fast 'surrogate' amenable for integration within real-time monitoring systems. By way of example, the proposed forecasting strategy is retrospectively applied to a recent field monitoring case history where the observational method is used to update the input parameters of the data-driven surrogate.

14 **LIST OF NOTATIONS**

15	γ_f	Unit weight of supporting fluid.
16	γ_s	Soil unit weight.
17	λ	Dimensionless constant expressing the variation of undrained shear strength with
18		depth.
19	ρ	Gradient of undrained shear strength with depth.
20	$e(n)$	Error of an output neuron on the n -th training example.
21	F	Factor of safety against excavation collapse.
22	H	Depth of excavation.
23	h_f	Height of supporting fluid (from internal excavation level).
24	k	Number of folds used in the cross-validation training process.
25	MSE	Mean squared error.
26	N_u	Undrained stability number.
27	R	Excavation radius.
28	s_{u0}	Undrained shear strength at ground level.
29	$s_u(z)$	Undrained shear strength at depth z .
30	x	Input variable for artificial neural network.
31	$y(n)$	Target output variable for the n -th training example.
32	$\hat{y}(n)$	Predicted output variable for the n -th training example.
33	z	Depth below ground level.

INTRODUCTION

The rapid expansion of urban areas promotes the need to exploit underground space and highlights the sustained importance of deep excavation works (O'Dwyer et al. 2018, 2019). In particular, deep large-diameter circular excavations and shafts are increasingly employed for underground developments (Sheil and Templeman 2021, Templeman et al. 2021). The use of strutting or construction fluids is a common means of providing additional support to maintain excavation stability until a more permanent structure is installed/constructed (Royston et al. 2020). The stability of these excavations is a critical design concern to ensure safe and efficient construction as well as the prevention of damage to existing nearby infrastructure.

The stability of vertical cuts associated with plane strain problems has been considered by several investigators. Morgenstern and Amir-Tahmasseb (1965) presented an analysis of a number of 'slips' that were observed during the construction of a slurry-supported trench excavation in Pierre-Bénite, France. An impervious boundary was observed to develop between the slurry and surrounding soil allowing a hydrostatic force to be exerted on the walls of the trench. Fox (2004) developed analytical solutions for the analysis of the stability of slurry trenches in homogeneous cohesive and cohesionless soils. That study highlighted the ability of closed-form analytical solutions to accurately capture field behaviour. Filz et al. (2004) investigated, using closed-form expressions, global and local excavation stability as a function of filter cake formation. Those authors noted that the effectiveness of support fluids is almost entirely governed by their ability to form a filter cake. More recently, Li et al. (2013) developed a horizontal slice method for the analysis of a slurry trench.

Bjerrum and Eide (1956) represents one of the earliest analyses of the stability of a circular (strutted) excavation in clay, using analytical solutions to capture basal failure observed in fourteen case histories. Finite element analysis has been widely used for the analysis of unsupported circular excavation stability (Sloan 1982, Griffiths and Koutsabeloulis 1985, Pastor and Turgeman 1982). Using upper-bound solutions, Britto and Kusakabe (1982, 1983) reported that wall failure is the most common mode of failure rather than base or combined

61 wall-base failure mechanisms for unsupported circular excavations. More recently, limit
62 analysis has become an increasingly popular analysis tool for this problem (e.g. Lyamin and
63 Sloan 2002a, Khatri and Kumar 2010, Kumar and Chakraborty 2012, Kumar et al. 2014).
64 Zhang et al. (2018) noted that one of the main benefits of these techniques is the use of
65 adaptive mesh strategies to reveal soil failure mechanisms.

66 While the stability of circular excavations has been well-researched, the behaviour of slurry-
67 supported excavations has received a lot less attention in the literature even though they are
68 very common in the construction industry. Uncertainties associated with the design and
69 construction of fluid-supported circular excavations include soil properties, support fluid
70 properties and excavation geometry. Traditionally, these uncertainties are accounted for using
71 often excessively conservative safety factors, selected based on engineering judgement
72 and/or accumulated experience. An alternative strategy that has the potential to save cost and
73 time and create safer working conditions is the 'observational method' first proposed by Peck
74 (1969). A prerequisite for the use of the observational method, however, is timely feedback of
75 information gleaned from the monitored data (Sheil et al. 2020).

76 Excavation collapse forecasting using stability charts is a manual and time-consuming process
77 as it requires the engineer to process monitored data and generate safety factor estimates on
78 an *ad-hoc* basis. Capturing these stability charts within a data-driven 'surrogate' is an
79 expedient means of incorporating sophisticated numerical analyses into monitoring systems
80 to generate stability predictions. For slurry supported excavations, this allows stability
81 forecasts to be generated 'on-the-fly' based on the current excavation geometry and support
82 fluid conditions. To this end, this paper explores a hybrid approach for forecasting circular
83 excavation collapse in undrained soil by combining the benefits of both physics-based and
84 data-driven modelling. Finite element limit analysis (FELA) is first undertaken towards the
85 development of a numerical (physics-based) database of stability numbers derived from 1,980
86 separate analyses. An artificial neural network (ANN) is used to 'learn' the numerical data to
87 act as fast FELA 'surrogates' (data-driven) for implementation in real-time monitoring

activities. By way of example, the proposed strategy is retrospectively applied to a recent field monitoring case history where the observational method is used to update the input parameters of the ANN surrogate.

A HYBRID APPROACH FOR REAL-TIME FORECASTING

Forecasting, or forward modelling, can be broadly categorized as either data-driven or physics-based. Data-driven approaches use information from previously acquired ('training') data to identify the characteristics of the currently measured state towards predicting future trends e.g. Sheil et al. (2020a, 2020b). However, this approach to forecasting has significant limitations including (a) data-hungry models, (b) inability to extrapolate outside the parameter space of the training data and (c) lack of explanatory power and therefore an inability to elucidate the underlying physics of the problem (Sheil 2021). In contrast, physics-based approaches adopt a theoretical model to describe the behavior of the system. One of the greatest drawbacks of these approaches is the cost of manually developing multiple simulations which has inhibited their implementation within real-time monitoring systems. In this paper, a 'hybrid' framework is proposed to combine the benefits of both types of modelling. A data-driven algorithm is used to 'learn' the behavior of a physics-based (FELA) model by developing a database of likely inputs and their numerically predicted outputs (see Fig. 1). This exercise creates a data-driven 'surrogate' of the numerical model amenable for deployment within a real-time monitoring system.

NUMERICAL DATABASE DEVELOPMENT

Problem definition

The soil parameters and excavation geometry considered in this study are illustrated in Fig. 2. The radius of the circular excavation is R and the depth is H . The excavation is assumed to be filled to a height h_f with support fluid of unit weight γ_f . In this study, excavation collapse

loads are sought so a factor of safety, F , of 1.0 is adopted in the numerical analyses. For the case where $h_f = H$, the undrained stability number, N_u , can be determined as follows (Whitlow 1990):

$$N_u = \frac{(\gamma_s - \gamma_f)HF}{s_{u0}} \quad (1)$$

where γ_s is the total unit weight of the surrounding soil and s_{u0} is the undrained shear strength at ground level. However, h_f is not always equal to H in practice due to potential infiltration of the support fluid through the surrounding soil. The range $0 \leq h_f \leq H$ is therefore considered in this study where $h_f = 0$ represents an unsupported excavation. The following dimensionless expression has therefore been adopted for N_u in lieu of equation (1):

$$N_u = \left(\frac{\gamma_s H - \gamma_f h_f}{s_{u0}} \right) F \quad (2)$$

Finite element limit analysis

The numerical database was developed using the finite element limit analysis program Optum G2 (Optum CE, 2016). Axisymmetric conditions were assumed for the majority of the analyses to explore the role of the excavation height-to-radius ratio (H/R) on excavation stability. A limited number of analyses were also completed assuming plane strain conditions, representing $H/R = 0$, as an extreme case. For each problem, an analysis was conducted using strict lower-bound (LB) and upper-bound (UB) plasticity solutions. The LB analyses used triangular elements with a linear variation in stresses between corner nodes such that yield conditions are enforced at the three corner nodes. The UB analyses used triangular elements with quadratic interpolation of displacements and linear interpolation of stresses within each element. The LB and UB analyses are subsequently cast as an optimisation problem which is solved using second order cone programming. This process allows a rigorous bracketing of the exact collapse loads where the error can be defined as follows:

$$error(\%) = \frac{UB - LB}{0.5 \times (UB + LB)} \quad (3)$$

In all analyses the error was less than 1.5% and the final collapse loads were obtained by averaging the LB and UB collapse multipliers at the end of the analysis. Each model was initially uniformly discretised with 1000 elements. The total number of elements at the end of the analysis varied up to a maximum of 6000 elements after six rounds of adaptive meshing based on shear dissipation rates. Sample meshes before and after adaptive remeshing are provided in Fig. 3 where the updated mesh can be used to reveal the excavation collapse mechanism. Further information on FELA procedures is available in Sloan (1988, 1989), Lyamin and Sloan (2002a, 2002b), Makrodimopoulos and Martin (2005, 2006, 2007, 2008), Martin (2011).

Modelling preliminaries

The parameters considered in the modelling are listed in Table 1. A value of 10 kN/m³ was maintained for γ_f in all analyses which represents a typical value adopted in practice to achieve effective filter cake formation (Poh and Wong 1998; Ng and Yan 1999; Li et al. 2009; Royston et al. 2020). Hydrostatic conditions were assumed for the slurry pressure which was therefore applied as a distributed load along the internal surface of the excavation, as shown in Fig. 2. The soil was modelled as an elastic-plastic Tresca material with an undrained shear strength profile defined as follows:

$$s_u(z) = s_{u0} + \rho z \quad (4)$$

where $s_u(z)$ is the undrained shear strength at a particular depth z below ground level and ρ is the increment of shear strength with depth. The undrained shear strength profile is characterised in terms of a dimensionless constant, λ :

$$\lambda = \frac{\rho H}{s_{u0}} \quad (5)$$

where a value of $\lambda = 0$ indicates a uniform s_u profile and a positive value indicates a shear strength that increases linearly with depth. The width of the soil domain was taken as $2.5R$ and the depth of the domain was taken as $2H$ to comfortably contain the soil failure mechanism for all soil/caisson parameter combinations considered. The lateral boundaries were restricted from movement normal to the respective surface, whereas the bottom boundary was restrained from movement in both directions. For the LB analyses, stress boundary conditions (normal and traction stresses) were determined from the depth below ground surface and user input of the soil unit weight and coefficient of lateral earth pressure.

Validation

The value of N_u for each analysis was determined using a strength reduction procedure. This approach provides an output of the minimum strength required to prevent collapse given a prescribed set of loads. The analysis proceeds by calculating a strength reduction factor by which the undrained shear strengths need to be reduced to attain a state of incipient collapse. For a given value of λ , this process provides the value of s_{u0} at failure ($s_{u0,f}$) for use in equation (2) to determine N_u .

Results from plane strain ($H/R = 0$) and axisymmetric ($H/R > 0$) FELA analyses are presented in Fig. 4 and compared to previously documented solutions to validate the present model and adopted methodology for determining N_u . It can be seen that the present results compare very well with those previously reported in the literature. In particular, the agreement with the results documented by Lyamin and Sloan (2002a) is to be expected given that the program used herein is a development of that work.

NUMERICAL RESULTS

Stability of slurry-supported circular excavations

The influence of H/R on N_u for a fully supported excavation is explored in Fig. 5. It can be observed that excavations with greater values of H/R exhibit significantly increased stability. For example, N_u is 186% greater for $H/R = 20$ compared to $H/R = 0$ for a uniform soil strength profile. This is due to a beneficial ‘arching effect’ arising from the development of compressive hoop stresses in the soil surrounding the excavation. Adaptive meshes and failure patterns corresponding to points a – h indicated on Fig. 5 are presented in Figs. 6(a) – 6(h) respectively. Considering first the $\lambda = 0$ results, increasing H/R causes the shape of the failure surface to transition from wall wedge failure to a combined wall–base rotational failure, as shown in Figs. 6(a) – 6(d). These results support the findings of Britto and Kusabe (1982), that a combined wall–base failure mechanism becomes critical for $H/R > 2.5$. It can also be seen that for values of H/R of 5 and 20, an increase in the strength gradient to $\lambda = 10$ prevents the failure mechanism from extending the full depth of the excavation (see Figs. 6(e) – 6(h)). This is because λ has a greater effect for higher values of H/R which can be observed if the data in Fig. 4 are recast as a function of λ (see Fig. 7).

Influence of support fluid head

The influence of the support fluid head on N_u is explored in Fig. 8. Firstly, the normalisation defined by equation (2) for N_u appears to be dependent on both h_i/H and γ_i/γ_s ; while N_u is consistent for the extreme cases of $h_i/H = 0$ and 1, N_u reduces for intermediate values of h_i/H . Furthermore, a discontinuity in the region $0.9 < h_i/H < 1$ can be observed for the $\gamma_i/\gamma_s = 0.9$ analyses. To further explore the cause of these reductions and the discontinuity, the failure mechanisms corresponding to points a – f are presented in Figs 9(a) – 9(f) respectively. For the $\gamma_i/\gamma_s = 0.5$ analyses, a reduction in h_i/H causes the failure surface to eventually shift upwards into the predominantly unsupported soil. In contrast, a reduction in h_i/H from 1 to 0.9 for the $\gamma_i/\gamma_s = 0.9$ analyses immediately causes failure to occur in the unsupported soil due to the higher relative weight of the support fluid. Further reductions in h_i/H causes the soil failure

surface to continue shifting downwards. It is worth remarking that modifications to the failure mechanism only occur when s_u varies with depth (i.e. $\lambda > 0$).

DEVELOPMENT OF DATA-DRIVEN SURROGATE

Artificial neural networks

An ANN is an information processing paradigm that draws inspiration from the operation of the human brain. A network consists of multiple interconnected layers of neurons, comprising a layer of input neurons, one or more layers of ‘hidden’ neurons that perform operations on the data, and a layer of output neurons. Transformation of the input data is performed by the artificial neurons through the application of a nonlinear function (known as the activation function) of the sum of weighted inputs (see Fig. 10). A large number of neural networks have been developed for a wide range of applications including radial basis function, Kohonen self-organising, recurrent, convolutional, and modular neural networks. In this paper, one of the simplest forms of ANN, a feedforward neural network, is adopted wherein the data travels in one direction, from input to output. After each complete iteration, termed ‘epochs’, the network output values are compared to the target values to produce an error measurement. The error, e , of an output neuron after the activation of the network on the n -th training example can be defined as:

$$e(n) = y(n) - \hat{y}(n) \quad (6)$$

Feedback of error through the network is known as ‘backpropagation’. The backpropagation algorithm is a nonlinear optimization process, known as gradient descent, which adjusts the weight and bias of each connection towards reducing the value of the error function. This process involves computing the gradient of the error function at each iteration step. Therefore, the continuity and differentiability of the error function must be guaranteed. Once all the training data have been applied, the process is repeated either for a specified number of epochs or until a predetermined error threshold is achieved.

233

234 *Pre-processing of numerical input data*

235 The input feature variables for this study are listed in Table 2 and N_u is the only output variable.
236 All data were pre-processed to maximise the efficiency and performance of the learning
237 process and to ensure that the importance of the input variables is equalised. A ‘min-max
238 scaler’ (Masters, 1993) was adopted here to transform both the input and output variables.
239 This transformation, applied to an input variable x_i for example, can be defined as follows:

$$\frac{x_i - \min(x)}{\max(x) - \min(x)} \quad (7)$$

240

241 *Supervised learning process*

242 The learning framework adopted in this study is shown in Fig. 11. To establish an optimal
243 network, an 80–20 train–test split was applied randomly to the entire database of numerical
244 results (see Table 3). To provide a rigorous assessment of the training process and reduce
245 the likelihood of overfitting, k -fold cross validation was undertaken on the training data. Ten
246 folds were adopted in this study as this value has been shown empirically to yield test error
247 rate estimates that suffer neither from excessively high bias nor from very high variance
248 (Kohavi, 1995). This process involves randomly partitioning the training data into $k = 10$ folds;
249 sequentially, $k - 1$ folds are used for training the model whereas one fold is used for validation.
250 This process is repeated k times such that each fold is used as a validation set once. The
251 training error is then obtained by averaging the $k = 10$ validation errors. The error
252 measurement used for this work is the mean squared error (MSE) defined as follows:

$$MSE = \frac{1}{n/k} \sum_{i=1}^{n/k} (y_i - \hat{y}_i)^2 \quad (8)$$

253 where n is the total number of training samples and k is the number of folds used in the
254 cross-validation. The data-driven algorithms were developed using the Python 3.6 library

scikit-learn (Pedregosa et al., 2011). For the hyperparameter optimisation stage, a grid search approach was adopted where the MSE is computed for several different hyperparameter combinations.

In this study, a hyperbolic tangent sigmoid was adopted for the activation function while a gradient descent algorithm with fixed learning rate was selected for updating weights and biases. A learning rate of 1×10^{-4} was adopted while each ANN was trained for 1,000 epochs to achieve a minimum error. In this study, networks with one and two hidden layers each comprising one to twenty hidden neurons each were considered. The influence of the network architecture on the model performance is shown in Fig. 12. It can be seen that for models with at least four hidden neurons per layer, a network with two hidden layers outperforms a single hidden layer network. A two-layer network comprising five neurons each with hyperbolic tangent activation functions was therefore selected based on the results of the grid search optimisation process.

Verification of ANN surrogate

The ANN was re-fit to the training data using the optimal hyperparameters identified by the grid search optimization process. Comparisons between the ANN predictions and the target FELA values for both the training and 'unseen' testing data are presented in Figs. 13(a) and 13(b) respectively. The ANN provides excellent predictions of both the training and unseen testing data. An additional advantage of an ANN over alternative approaches, such as support vector regression and random forests, is increased interpretability where the trained model can be decomposed into its constituent closed-form equations and replicated in spreadsheet form, for example. This is also highly beneficial for deployment within real-time monitoring systems, avoiding the need for specific software and/or experience in programming. The present (trained) ANN can be disintegrated as follows:

$$N_u = 67.8 \tanh(-1.13 \tanh H_{21} + 2.25 \tanh H_{22} - 0.29 \tanh H_{23} + 0.92 \tanh H_{24} + 2.47 \tanh H_{25} - 0.15) \quad (9)$$

where:

$$\begin{bmatrix} H_{21} \\ H_{22} \\ H_{23} \\ H_{24} \\ H_{25} \end{bmatrix} = [A] \begin{bmatrix} H_{11} \\ H_{12} \\ H_{13} \\ H_{14} \\ H_{15} \end{bmatrix} + [B] \quad (10)$$

$$\begin{bmatrix} H_{11} \\ H_{12} \\ H_{13} \\ H_{14} \\ H_{15} \end{bmatrix} = \tanh \left([C] \begin{bmatrix} H/R \\ \gamma_f/\gamma_s \\ \lambda \\ h_f/H \end{bmatrix} + [D] \right) \quad (11)$$

Matrices A and C and vectors B and D are provided in Appendix I. In the equations above, the coefficients have been modified to allow for a direct input of the unscaled input and output parameter values.

EXAMPLE APPLICATION

By way of example, the proposed hybrid forecasting strategy is retrospectively applied to a recent field monitoring case history described by Royston (2018a, 2018b) involving the construction of a 20 m deep, 13 m external diameter reinforced concrete shaft (see Fig. 14). Local geology comprises 20 m of soft normally-consolidated Blue Lias clay, underlain by firm mudstone. Undrained shear strengths for the Blue Lias clay are presented in Fig. 15 and were determined from cone penetration tests using a cone factor of 19 (calibrated using in-house triaxial tests on block samples taken from site).

The construction process involves a complex system of concurrent casting of the concrete walls and excavation of the soil inside and beneath the caisson (Royston et al. 2016, Sheil et al. 2018, Royston et al. 2020). A 60° tapered ‘cutting face’ was adopted at the base of the wall to provide control during caisson sinking with the self-weight of the concrete walls used as

kentledge. The caisson was founded 20 m below ground on firm mudstone strata. A key feature of that construction process was the use of a 70 mm annulus encircling the structure, which was created by the steel leading edge, as shown in Fig. 16. The annulus was filled with support fluid to maintain the stability of the external excavation. The fluid-supported excavation radius, R , was therefore 6.57 m. The proposed monitoring strategy can be outlined as follows:

- I. Real-time measurements of the shaft penetration process are used to update the 'current' value of H (and therefore H/R) while measurements of the lubricant pressures in the annulus are used to infer h_f and γ_f , assuming hydrostatic conditions e.g. Sheil et al. (2018), Royston (2018b).
- II. Soil parameters s_{u0} and λ are determined for the region $0 \leq z \leq H$ through fitting a linear relationship to the measured undrained strength profile shown in Fig. 15. A value of 19 kN/m³ was determined for γ_s from laboratory tests.
- III. Equations (9) – (11) are used to compute the current value of N_u .
- IV. The current factor of safety, F , against collapse is determined using equation (2).

The annulus was fully supported throughout the construction project, based on site measurements and observations (Royston 2018b) while γ_f was measured as 10 kN/m³. The measured excavation depth and predictions of N_u and the factor of safety are plotted as a function of time in Fig. 17. Although N_u increases during construction due to the beneficial arching effect, the safety factor reduces significantly, approaching a value of 1.06 towards the end of construction ($H = 20$ m). While these predictions confirm that the excavation / annulus remained stable throughout the construction project, they indicate that annulus collapse would have occurred had the excavation been approximately 6 m deeper.

LIMITATIONS OF MODELLING

Assumptions imposed in the present modelling have important implications for future applications of the developed data-driven model. This study has explored undrained excavation collapse and therefore consolidation of the soil is not accounted for. A separate assessment of drained excavation collapse should be undertaken if the construction duration is sufficient to allow significant consolidation of the soil to occur. In this study, the soil is modelled as a rigid-plastic material. In reality, post-peak reduction in soil strength arising from significant soil deformations is possible, potentially accompanied by non-ductile material response. Finally, this study assumes that the supporting fluid transfers full hydrostatic pressure to the excavation soil surface. However, the effectiveness of supporting fluids are highly dependent on filter cake formation and adequate assessment and verification of filter cake formation is warranted in practice.

CONCLUSIONS

This paper has described the development of a hybrid monitoring strategy to provide early collapse warning for circular excavations by combining the benefits of both physics-based and data-driven modelling. A database of stability numbers for both unsupported and fluid-supported circular excavations was first developed using finite element limit analysis, considering the influence of excavation geometry, soil strength profile and support fluid properties. A data-driven artificial neural network, amenable for integration within real-time monitoring systems, was subsequently used to learn the numerical output to develop a (fast) 'surrogate'. The following conclusions can be drawn from the work:

- (a) Excavation geometry has a significant influence on the stability of both fluid-supported and unsupported circular excavations. This is due to the development of compressive hoop strains in the surrounding soil which leads to a beneficial arching effect. The failure mechanisms determined from the numerical modelling can be broadly categorized as either wall failure or combined wall-base failure, corresponding to excavations with low and high excavation height-to-radius ratios respectively.

- (b) For a soil strength profile that increases linearly with depth, the present study revealed the potential for the failure mechanism to shift upwards into the weaker soil depending on the excavation geometry. A reduction in the height of support fluid was also shown to promote an upward shift in the location of the failure mechanism, particularly if the relevant fluid-to-soil unit weight is high.
- (c) An artificial neural network was adopted to develop a surrogate of the developed finite element limit analysis model. The ANN provided excellent predictions of the finite element limit analysis training and testing data. An ANN is also desirable for its interpretability where the trained model can be easily disintegrated into its constituent closed-form expressions
- (d) An excavation collapse forecasting strategy using an ANN-based surrogate was proposed. By way of example, the proposed strategy was retrospectively applied to a recent field monitoring case history where the ANN input parameters were updated according to the observational method. The results show an exciting potential for the incorporation of data-driven algorithms within monitoring systems to generate collapse forecasts in real time.

ACKNOWLEDGEMENTS

This project was funded by the Royal Academy of Engineering under the Research Fellowship scheme. The author gratefully acknowledges the support and input from Ward and Burke Construction Ltd.

DATA AVAILABILITY STATEMENT

Some or all data, models, or code that support the findings of this study are available from the corresponding author upon reasonable request.

REFERENCES

- Bjerrum, L. and O. and Eide. 1956. "Stability of strutted excavations in clay." *Géotechnique* 6 (1): 32-47. <https://doi.org/10.1680/geot.1956.6.1.32>.
- Britto, A. M. and O. Kusakabe. 1982. "Stability of unsupported axisymmetric excavations in soft clay". *Géotechnique* 32 (3): 261–270. <https://doi.org/10.1680/geot.1982.32.3.261>.
- Britto, A. M. and O. Kusakabe. 1983. "Stability of axisymmetric excavations in clays." *Journal of Geotechnical Engineering ASCE* 109 (5): 666-681. [https://doi.org/10.1061/\(ASCE\)0733-9410\(1983\)109:5\(666\)](https://doi.org/10.1061/(ASCE)0733-9410(1983)109:5(666)).
- Filz, G. M., T. Adams and R. R. Davidson. 2004. "Stability of long trenches in sand supported by bentonite-water slurry." *Journal of Geotechnical and Geoenvironmental Engineering ASCE* 130 (9): 915-921. <https://doi.org/10.1007/s11771-014-2350-4>.
- Fox, P. J. 2004. "Analytical solutions for stability of slurry trench." *Journal of Geotechnical and Geoenvironmental Engineering ASCE* 130 (7): 749-758. [https://doi.org/10.1061/\(ASCE\)1090-0241\(2004\)130:7\(749\)](https://doi.org/10.1061/(ASCE)1090-0241(2004)130:7(749)).
- Griffiths, D. V. and N. Koutsabeloulis. 1985. "Finite element analysis of vertical excavations." *Computers and Geotechnics* 1 (3): 221-235. [https://doi.org/10.1016/0266-352X\(85\)90025-4](https://doi.org/10.1016/0266-352X(85)90025-4).
- Khatri, V. N. and J. Kumar. 2010. "Stability of an unsupported vertical circular excavation in clays under undrained condition." *Computers and Geotechnics* 37 (3): 419–424. <https://doi.org/10.1016/j.compgeo.2009.11.001>.
- Kohavi, R. 1995. A study of cross-validation and bootstrap for accuracy estimation and model selection. In *International Joint Conference on Artificial Intelligence, Montreal, Canada*. Morgan Kaufmann Publishers Inc. CA, USA, vol. 14, pp. 1137-1145.
- Kumar, J. and D. Chakraborty. 2012. "Stability number for an unsupported vertical circular excavation in c - ϕ soil." *Computers and Geotechnics* 39: 79–84. [https://doi.org/10.1061/\(ASCE\)GT.1943-5606.0001118](https://doi.org/10.1061/(ASCE)GT.1943-5606.0001118).
- Kumar, J., M. Chakraborty and J. P. Sahoo. 2014. "Stability of unsupported vertical circular excavation." *Journal of Geotechnical and Geoenvironmental Engineering ASCE* 140 (7): 04014028. [https://doi.org/10.1061/\(ASCE\)GT.1943-5606.0001118](https://doi.org/10.1061/(ASCE)GT.1943-5606.0001118).
- Li, Y.-C., P. Qian, P. J. Cleall, W.-M. Chen H. and Ke. 2013. "Stability analysis of slurry trenches in similar layered soils." *Journal of Geotechnical and Geoenvironmental Engineering ASCE* 139 (12): 2104-2109. [https://doi.org/10.1061/\(ASCE\)GT.1943-5606.0000958](https://doi.org/10.1061/(ASCE)GT.1943-5606.0000958).
- Li, Y., F. Emeriault, R. Kastner and Z. X. Zhang. 2009. "Stability analysis of large slurry shield-driven tunnel in soft clay." *Tunnelling and Underground Space Technology* 24 (4): 472-481. <https://doi.org/10.1016/j.tust.2008.10.007>.

Lyamin, A. V. and S. W. Sloan. 2002a. "Upper bound limit analysis using linear finite elements and non-linear programming." *International Journal for Numerical and Analytical Methods in Geomechanics* 26 (2): 181–216. <https://doi.org/10.1002/nag.198>.

Lyamin, A.V. and Sloan, S.W., 2002. Lower bound limit analysis using non-linear programming. *International Journal for Numerical Methods in Engineering* 55 (5): 573-611. <https://doi.org/10.1002/nme.511>.

Makrodimopoulos, A. and Martin, C.M., 2005. Limit analysis using large-scale SOCP optimization. In *Proc. 13th Nat. Conf. of UK Association for Computational Mechanics in Engineering, Sheffield*, pp. 21-24.

Makrodimopoulos, A. and Martin, C.M., 2006. Lower bound limit analysis of cohesive-frictional materials using second-order cone programming. *International Journal for Numerical Methods in Engineering* 66 (4): 604-634. <https://doi.org/10.1002/nme.1567>.

Makrodimopoulos, A. and Martin, C.M., 2007. Upper bound limit analysis using simplex strain elements and second-order cone programming. *International journal for numerical and analytical methods in geomechanics* 31 (6): 835-865. <https://doi.org/10.1002/nag.567>.

Makrodimopoulos, A. and Martin, C.M., 2008. Upper bound limit analysis using discontinuous quadratic displacement fields. *Communications in Numerical Methods in Engineering* 24 (11): 911-927. <https://doi.org/10.1002/cnm.998>.

Martin, C.M., 2011. The use of adaptive finite-element limit analysis to reveal slip-line fields. *Géotechnique Letters* 1 (2): 23-29. <https://doi.org/10.1680/geolett.11.00018>.

Masters, T. 1993. *Practical neural network recipes in C++*. Academic Press, San Diego, CA.

Morgenstern, N. and I. Amir-Tahmasseb. 1965. "The stability of a slurry trench in cohesionless soils." *Geotechnique* 15 (4): 387-395. <https://doi.org/10.1680/geot.1965.15.4.387>.

Ng, C. W. W. and R. W. M. Yan. 1999. "Three-dimensional modelling of a diaphragm wall construction sequence." *Geotechnique* 49 (6): 825-834. <https://doi.org/10.1680/geot.1999.49.6.825>.

O'Dwyer, K.G., McCabe, B.A., Sheil, B.B. and Hernon, D.P. (2018) Blackpool South Strategy Project: analysis of pipe-jacking records, Proceedings of Civil Engineering Research in Ireland (CERI 2018), pp. 265-270.

O' Dwyer, K. G., B. A. McCabe and B. B. Sheil. 2019. "Interpretation of pipe-jacking and lubrication records for drives in silty sand." *Underground Space*. <https://doi.org/10.1016/j.undsp.2019.04.001>.

Optum CE (2016) *Optum G2*, Optum Computational Engineering, Newcastle, New South Wales, Australia.

- Pastor, J. and S. Turgeman. 1982. "Limit analysis in axisymmetrical problems: numerical determination of complete statical solutions." *International Journal of Mechanical Sciences* 24 (2): 95–117. [https://doi.org/10.1016/0020-7403\(82\)90041-8](https://doi.org/10.1016/0020-7403(82)90041-8).
- Peck, R. B. 1969. "Advantages and limitations of the observational method in applied soil mechanics." *Geotechnique* 19 (2): 171-187. <https://doi.org/10.1680/geot.1969.19.2.171>.
- Pedregosa, F., G. Varoquaux, A. Gramfort et al. 2011. "Scikit-learn: Machine learning in Python." *Journal of Machine Learning Research* 12: 2825-2830. <https://arxiv.org/abs/1201.0490>.
- Poh, T. Y. and I. H. Wong. 1998. "Effects of construction of diaphragm wall panels on adjacent ground: field trial." *Journal of Geotechnical and Geoenvironmental Engineering ASCE* 124 (8): 749-756. [https://doi.org/10.1061/\(ASCE\)1090-0241\(1998\)124:8\(749\)](https://doi.org/10.1061/(ASCE)1090-0241(1998)124:8(749)).
- Royston, R., B. Phillips, B. B. Sheil and B. W. Byrne. 2016. Bearing capacity beneath tapered blades of open dug caissons in sand. *Civil Engineering Research in Ireland (CERI), Galway, Ireland*.
- Royston, R. (2018a) Monitoring the construction of a large diameter caisson in clay. In *Proceedings of the 26th European Young Geotechnical Engineers Conference, Graz, Austria*.
- Royston, R. (2018b) Investigation of Soil-Structure Interaction for Large Diameter Caissons. D.Phil. thesis, University of Oxford.
- Royston, R., B. B. Sheil and B.W. Byrne. 2020. "Monitoring the construction of a large-diameter caisson in sand." *Proceedings of the ICE - Geotechnical Engineering*. <https://doi.org/10.1680/jgeen.19.00266>.
- Royston, R., Sheil, B.B. and Byrne, B.W., 2020. Undrained bearing capacity of the cutting face of large-diameter caissons. *Géotechnique*. Published online ahead of print. <https://doi.org/10.1680/jgeot.20.P.210>.
- Sheil, B., 2021. Prediction of microtunnelling jacking forces using a probabilistic observational approach. *Tunnelling and Underground Space Technology*, 109, p.103749.
- Sheil, B. B., R. Royston and B. W. Byrne. 2018. Real-Time Monitoring of Large-Diameter Caissons. In *Proceedings of China-Europe Conference on Geotechnical Engineering*, Springer, pp. 725-729.
- Sheil, B. B., S. K. Suryasentana and W. -C. Cheng. 2020. "Assessment of Anomaly Detection Methods Applied to Microtunneling." *Journal of Geotechnical and Geoenvironmental Engineering* 146 (9): 04020094. [https://doi.org/10.1061/\(ASCE\)GT.1943-5606.0002326](https://doi.org/10.1061/(ASCE)GT.1943-5606.0002326).
- Sheil, B.B., Suryasentana, S.K., Mooney, M.A. and Zhu, H., 2020a. Machine learning to inform tunnelling operations: recent advances and future trends. *Proceedings of the*

Institution of Civil Engineers-Smart Infrastructure and Construction. Published online ahead of print. <https://doi.org/10.1680/jsmic.20.00011>.

Sheil, B.B., Suryasentana, S.K., Mooney, M.A., Zhu, H., McCabe, B.A. and O'Dwyer, K.G., 2020. Discussion: Machine learning to inform tunnelling operations: recent advances and future trends. *Proceedings of the Institution of Civil Engineers-Smart Infrastructure and Construction* 173 (1): 180-181. <https://doi.org/10.1680/jsmic.2020.173.1.180>.

Sheil, B. and Templeman, J., 2021. Bearing capacity of large-diameter open caissons embedded in sand. *Géotechnique*. In press.

Sloan, S. W. 1982. *Numerical analysis of incompressible and plastic solids using finite elements* (Doctoral dissertation, University of Cambridge).

Sloan, S.W., 1988. Lower bound limit analysis using finite elements and linear programming. *International Journal for Numerical and Analytical Methods in Geomechanics* 12 (1): 61-77. <https://doi.org/10.1002/nag.1610120105>.

Sloan, S.W., 1989. Upper bound limit analysis using finite elements and linear programming. *International Journal for Numerical and Analytical Methods in Geomechanics* 13 (3): 263-282. <https://doi.org/10.1002/nag.1610130304>.

Templeman, J.O., Phillips, B.M. and Sheil, B.B., 2021. Cutting shoe design for open caissons in sand: influence on vertical bearing capacity. *Proceedings of the Institution of Civil Engineers-Geotechnical Engineering*. Published online ahead of print. <https://doi.org/10.1680/jgeen.20.00218>.

Whitlow, R. 1990. *Basic soil mechanics*. Longman Group UK Ltd, Essex, England.

Zhang, J., Y. Gao, T. Feng, J. Yang and F. Yang. 2018. "Upper-bound finite-element analysis of axisymmetric problems using a mesh adaptive strategy." *Computers and Geotechnics* 102: 148-154. <https://doi.org/10.1016/j.compgeo.2018.06.008>.

508 APPENDIX I – MATRICES FOR TRAINED ANN MODEL

509 $A = \begin{bmatrix} 1.34 & 0.11 & 1.83 & 2.04 & 0.28 \\ -0.67 & 1.28 & 0.17 & 0.98 & 4.88 \\ -1.79 & 0.14 & 0.87 & -0.96 & 0.15 \\ -1.37 & 0.16 & -0.41 & 1.18 & 1.65 \\ 1.34 & 3.67 & -1.89 & -1.21 & -3.66 \end{bmatrix}$

510 $B = \begin{bmatrix} -1.85 \\ 0.6 \\ -1.54 \\ -2.21 \\ -3.39 \end{bmatrix}$

511 $C = \begin{bmatrix} -0.29 & 0.6 & 0.38 & 5 \\ -0.02 & -34 & -0.15 & 31.2 \\ -0.28 & -0.60 & -0.9 & -3.3 \\ -0.24 & 0 & 0.78 & -3.6 \\ -0.03 & -31.6 & -0.18 & -316 \end{bmatrix} \times 10^{-1}$

512 $D = \begin{bmatrix} -0.13 \\ 0.63 \\ 0.62 \\ -0.29 \\ 6.64 \end{bmatrix}$

513

514

515

Table 1 Excavation / soil parameters considered in the development of the numerical database

Parameter	Value
Excavation depth (m)	10
Excavation height-to-radius ratio, H/R	0 (plane strain), 1.0, 2.5, 5, 10, 20
Normalised variation of undrained shear strength with depth, λ	0, 2.5, 5, 7.5, 10
Unit weight of supporting fluid, γ_f (kN/m ³)	10
Support fluid–soil weight ratio γ_f / γ_s	0.5, 0.6, 0.7, 0.8, 0.9, 1.0
Normalised slurry height, h_i/H	0 to 1.0 (in increments of 0.1)

Table 2 Input ‘feature’ variables used to develop an ANN surrogate of the present FELA model

No.	Feature
1	H/R
2	γ_f/γ_s
3	λ
4	h_i/H

Table 3 Details of the training–testing split used in the ANN learning process

Parameter		Training data	Testing data	Total
Samples		1584 (80%)	396 (20%)	1980
H/R	Max	20	20	20
	Mean	6.39	6.54	6.42
	Min	0	0	0
γ_f/γ_s	Max	1	1	1
	Mean	0.75	0.76	0.75
	Min	0.5	0.5	0.5
λ	Max	10	10	10
	Mean	4.99	5.03	5
	Min	0	0	0
h_i/H	Max	1	1	1
	Mean	0.49	0.52	0.5
	Min	0	0	0
N_u	Max	67.35	67.6	67.8
	Mean	18.93	18.46	18.83
	Min	0	0	0

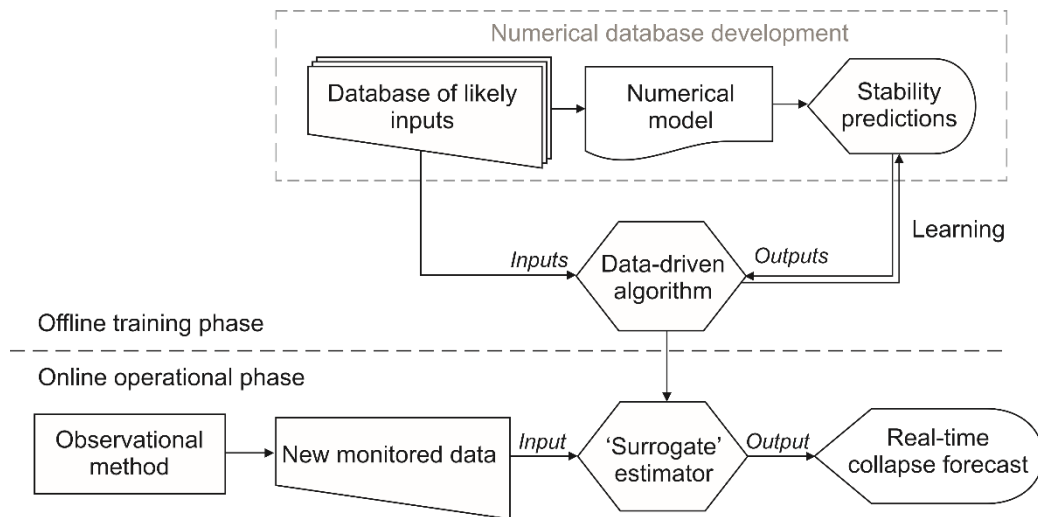


Fig. 1 Illustration of physics-based forecasting of circular excavation collapse using a surrogate estimator

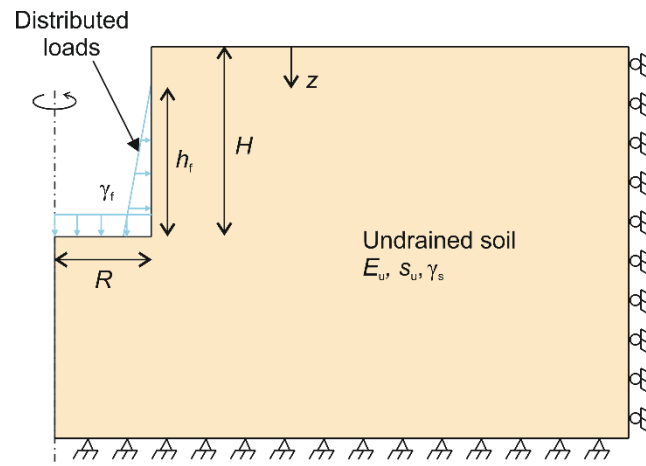


Fig. 2 Problem definition (axisymmetric case)

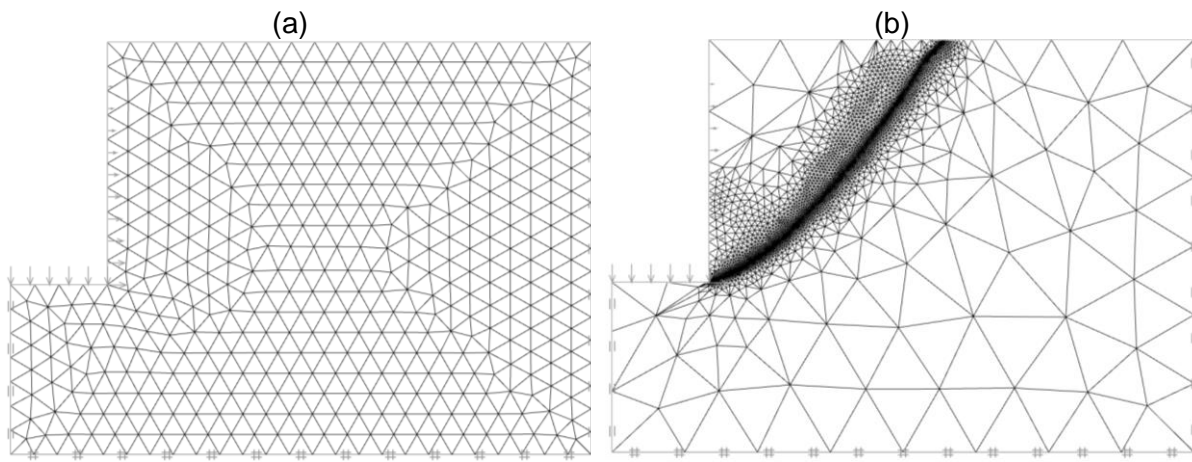


Fig. 3 Sample mesh (a) before and (b) after adaptive remeshing; $\lambda = 0$, $H/R = 0$ (plane strain), $h_f/H = 1$

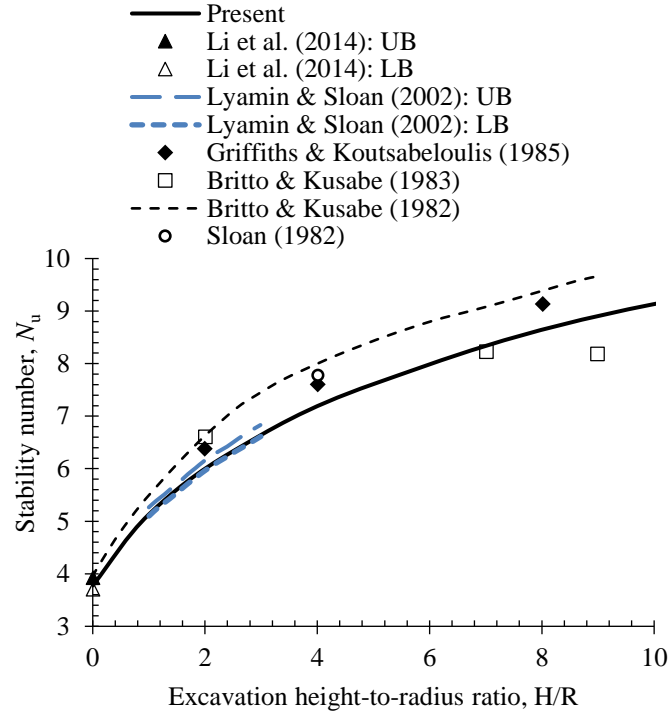


Fig. 4 Influence of excavation geometry on the undrained stability number, N_u , for an unsupported circular excavation predicted by the present FELA model compared to previously published stability numbers; $H/R = 0$ (plane strain)

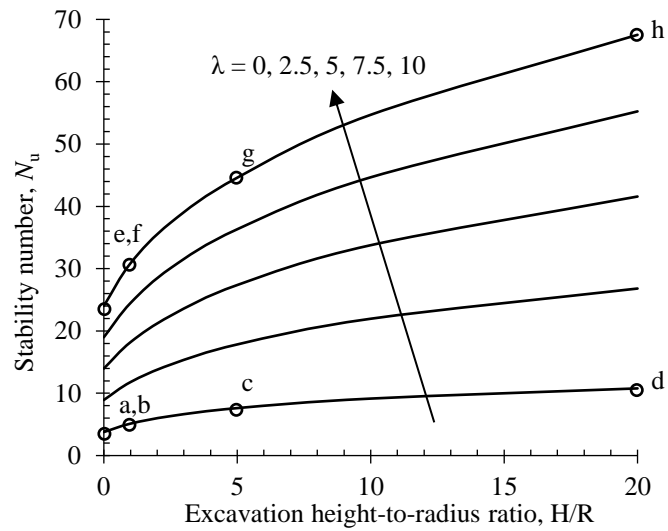


Fig. 5 FELA predictions of the influence of excavation geometry (H/R) on the undrained stability number for a fully supported excavation ($h_t / H = 1$); $\gamma_t / \gamma_s = 0.5$

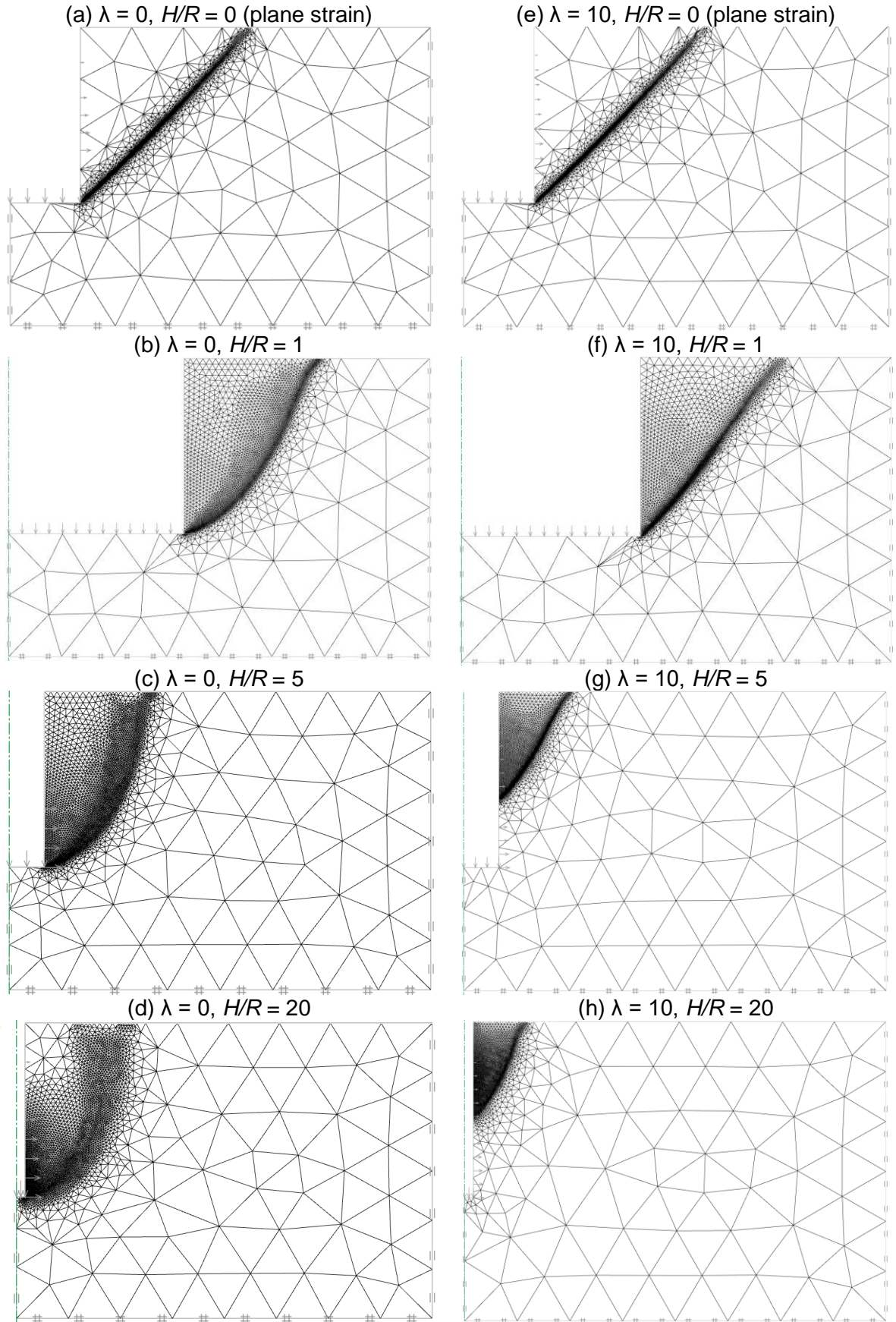


Fig. 6 FELA predictions of the influence of excavation geometry (H/R) on adaptive meshes and failure patterns for a slurry-supported circular excavation; $h_t / H = 1$, $\gamma_t / \gamma_s = 0.5$

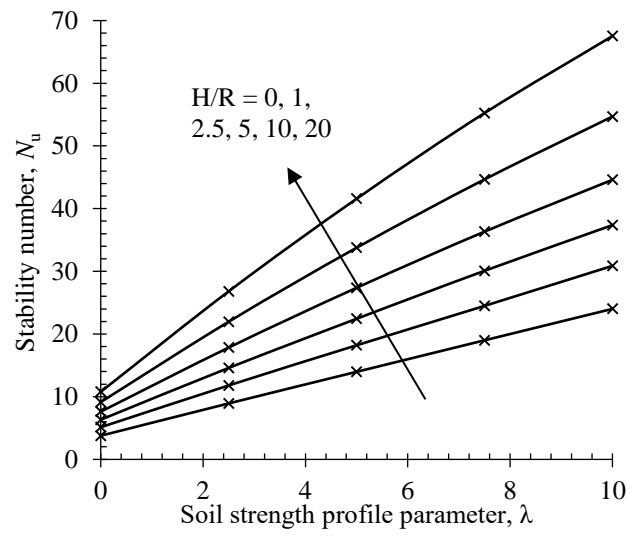


Fig. 7 FELA predictions of the influence of λ on the undrained stability number for a range of excavation geometries; $\gamma_t/\gamma_s = 0.5$, $h_t / H = 1$

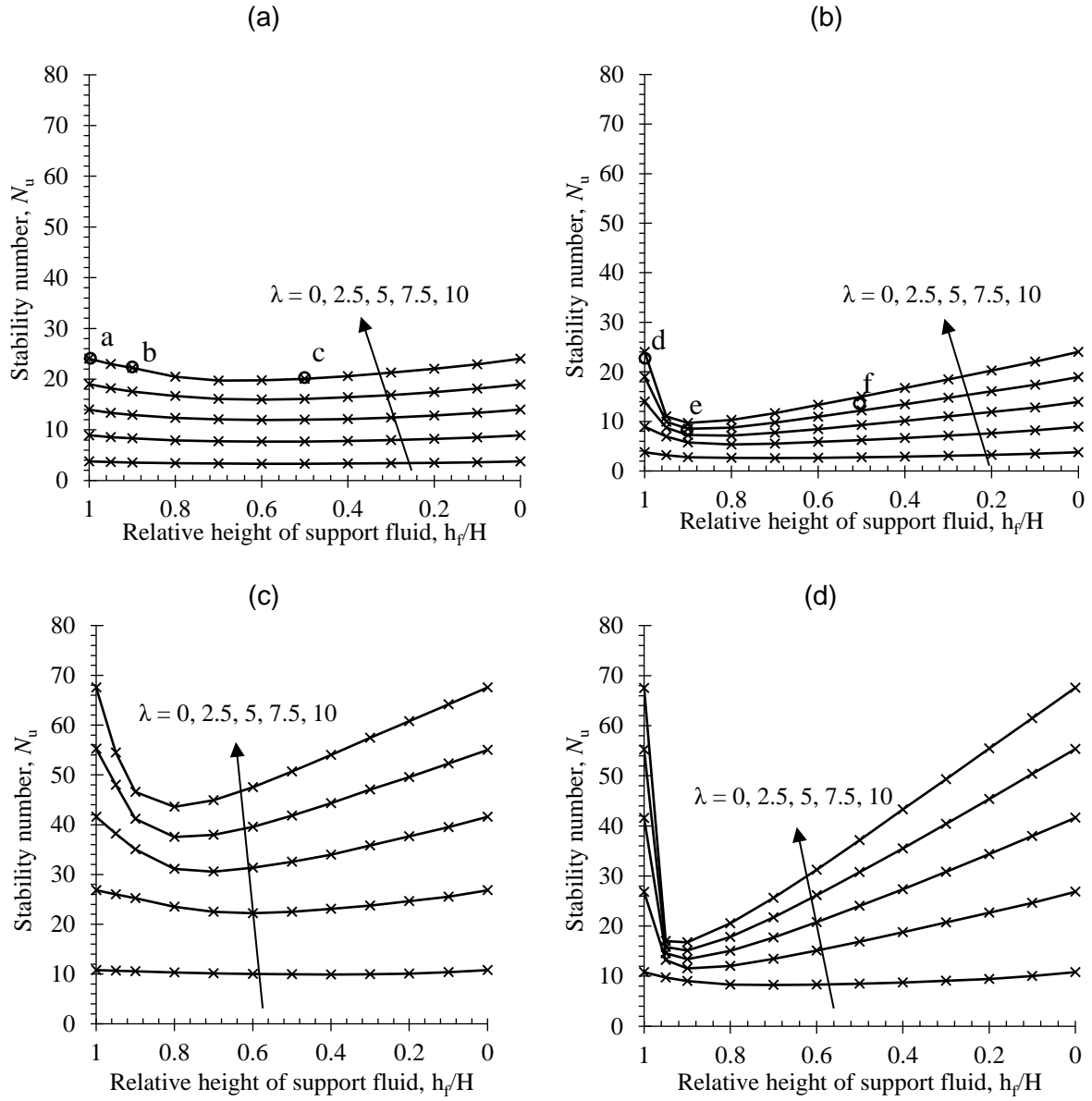


Fig. 8 FELA predictions of the influence of the relative height of support fluid on the undrained stability number for different fluid-to-soil weight ratios and soil strength profiles: (a) $H/R = 0$ (plane strain), $\gamma_t/\gamma_s = 0.5$, (b) $H/R = 0$, $\gamma_t/\gamma_s = 0.9$, (c) $H/R = 20$, $\gamma_t/\gamma_s = 0.5$, (d) $H/R = 20$, $\gamma_t/\gamma_s = 0.9$

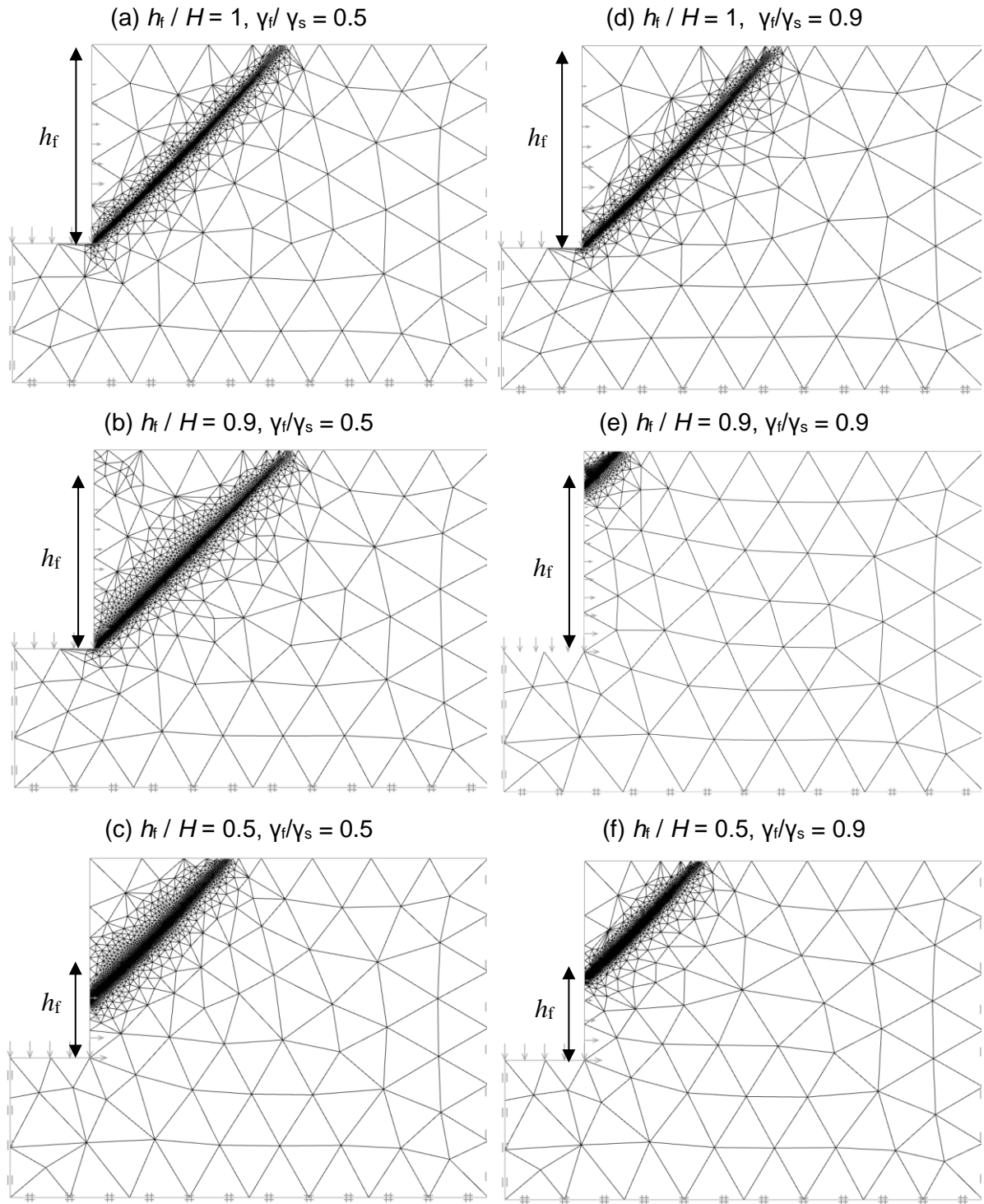


Fig. 9 Influence of support fluid head on failure patterns, revealed using FELA adaptive meshes; $H/R = 0, \lambda = 10$

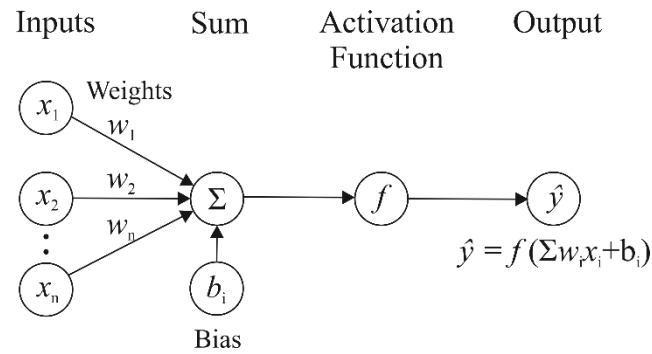


Fig. 10 Structure of a single artificial neuron showing mathematical operations performed on the input data

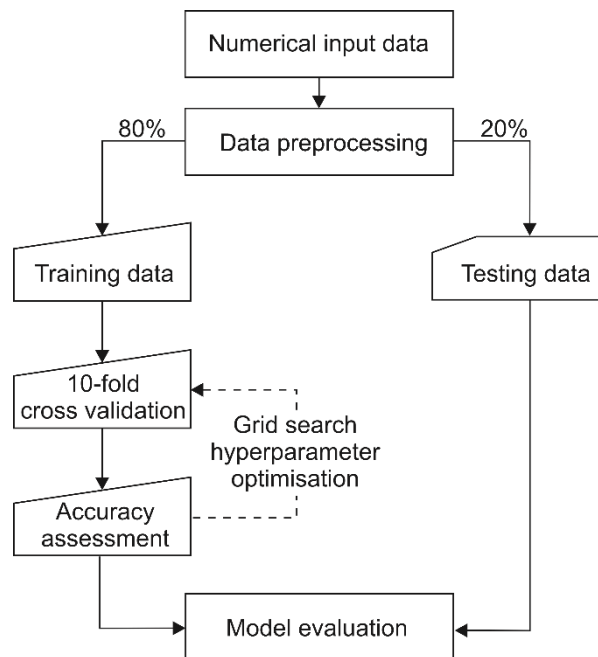


Fig. 11 Supervised learning process adopted for the development of the ANN surrogate

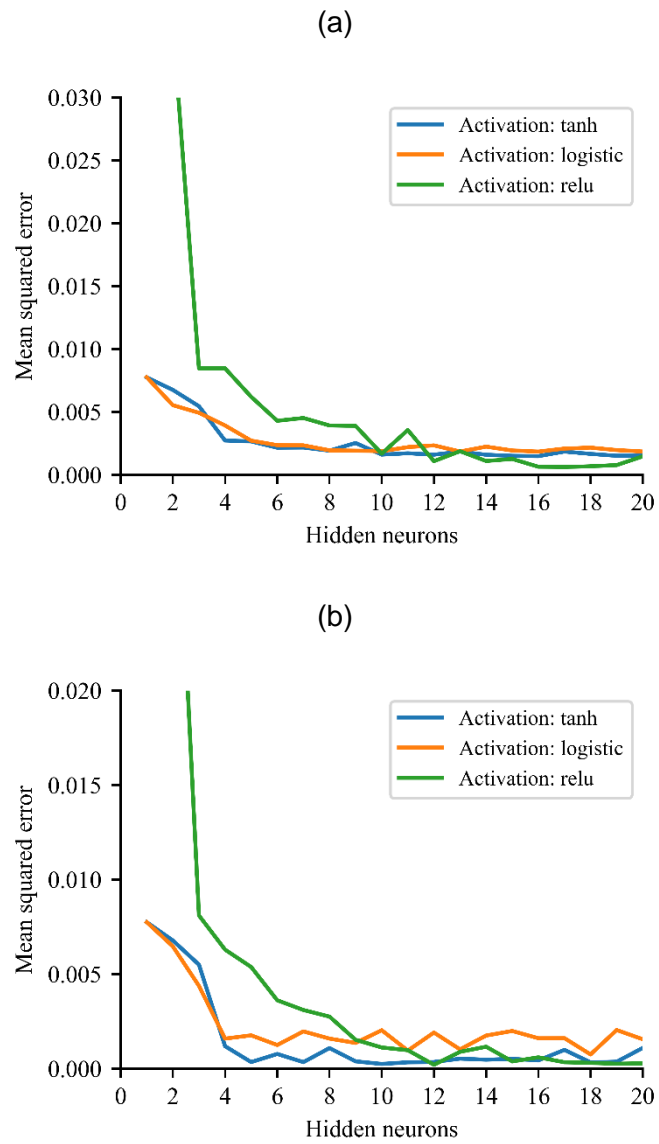


Fig. 12 Influence of ANN activation function and number of hidden neurons on the mean squared error of the output during training: (a) single-layer network, (b) two-layer network

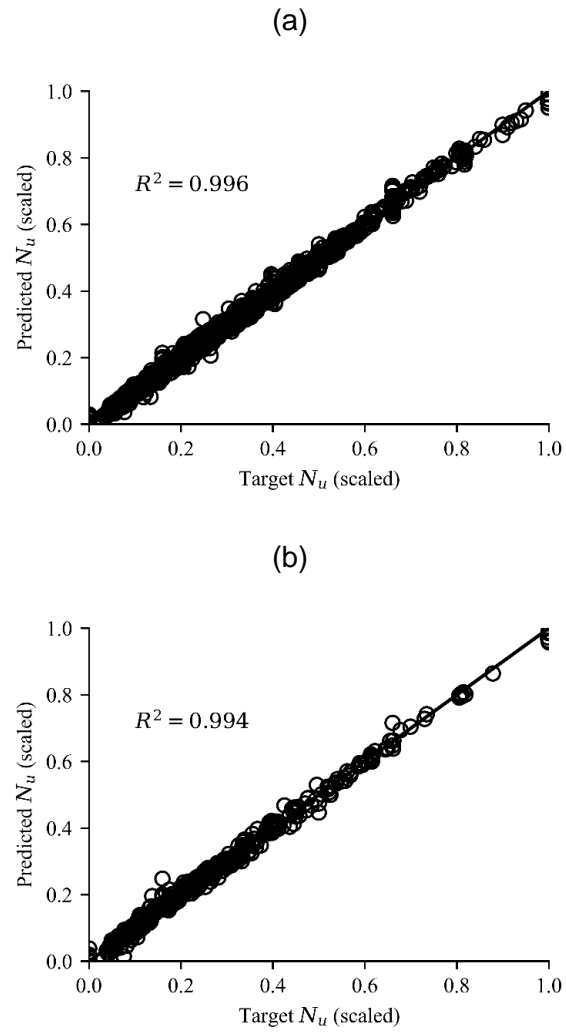


Fig. 13 Comparison between FELA results and predictions determined using the fitted ANN surrogate: (a) training data, (b) unseen testing data (see Table 3 for split)

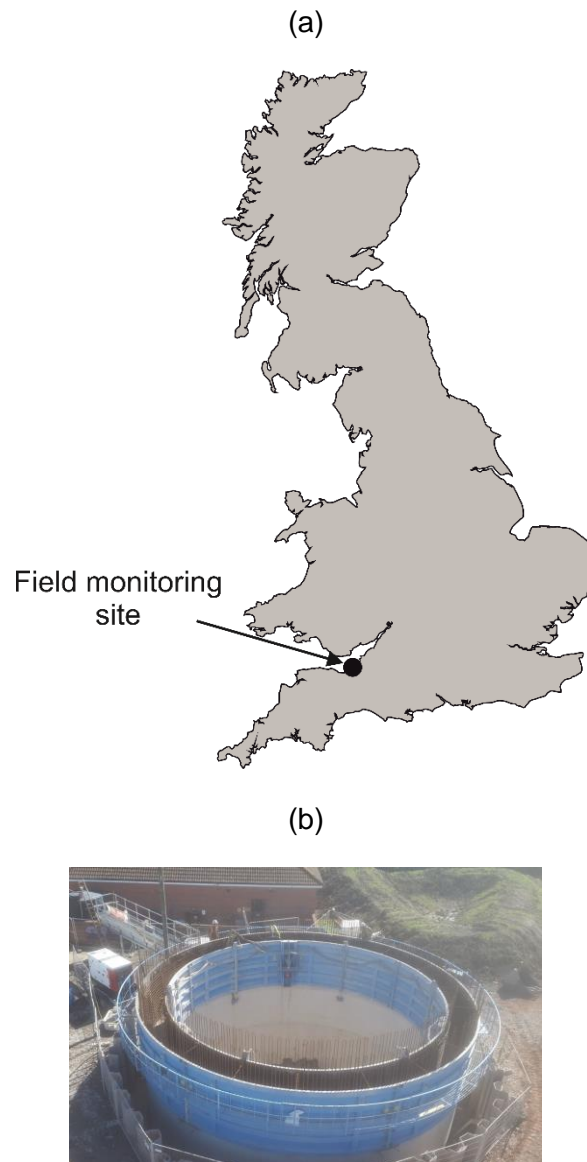


Fig. 14 (a) Field monitoring site at Bridgewater, UK and (b) large-diameter reinforced concrete caisson under construction

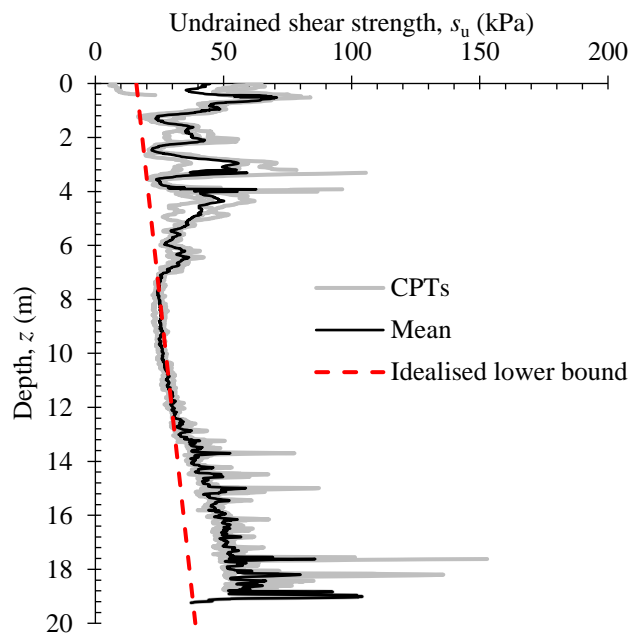


Fig. 15 Measurements of s_u derived from cone penetration tests (CPTs) at Bridgewater, UK (Royston 2018)

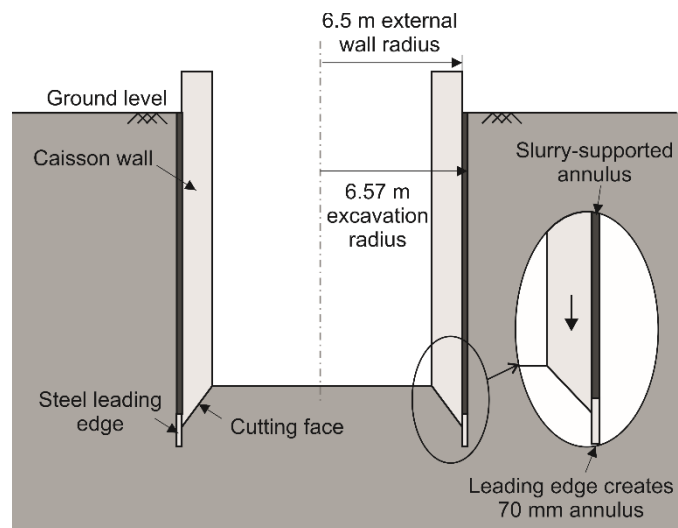


Fig. 16 Schematic illustration of cross-section through caisson showing wall and excavation geometry

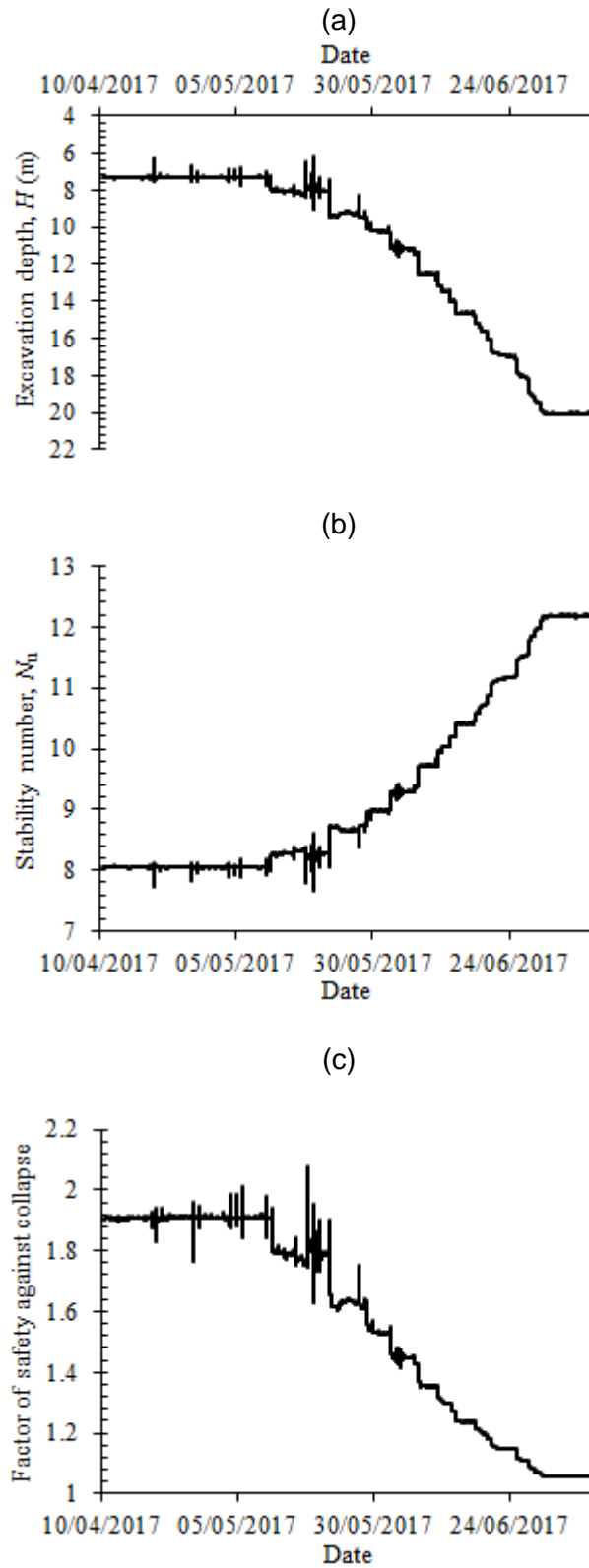


Fig. 17 Application of the proposed data-driven monitoring strategy to Bridgewater case history: (a) excavation depth time history, (b) N_u time history and (c) factor of safety time history